npj | quantum materials

www.nature.com/npjquantmats

ARTICLE OPEN

Check for updates

Second order Zeeman interaction and ferroquadrupolar order in $TmVO_4$

I. Vinograd[1], K. R. Shirer[2], P. Massat[3], Z. Wang[1], T. Kissikov[1], D. Garcia[1], M. D. Bachmann[3], M. Horvatić[4], I. R. Fisher[3] and N. J. Curro[1]✉

$TmVO_4$ exhibits ferroquadrupolar order of the Tm 4f electronic orbitals at low temperatures, and is a model system for Ising nematicity. A magnetic field oriented along the *c*-axis constitutes a transverse effective field for the quadrupolar order parameter, continuously tuning the system to a quantum phase transition as the field is increased from zero. In contrast, in-plane magnetic fields couple to the order parameter only at second order, such that orienting along the primary axes of the quadrupole order results in an effective longitudinal field, whereas orienting at 45 degrees results in a second effective transverse field. Not only do in-plane fields engender a marked in-plane anisotropy of the critical magnetic and quadrupole fluctuations above the ferroquadrupolar ordering temperature, but in-plane transverse fields initially enhance the ferroquadrupolar order, before eventually suppressing it, an effect that we attribute to admixing of the higher crystalline electric field levels.

npj Quantum Materials (2022)7:68 ; https://doi.org/10.1038/s41535-022-00475-1

INTRODUCTION

Electronic nematic order refers to a state in which low energy electronic degrees of freedom drive a crystal to spontaneously break discrete rotational symmetry without simultaneously breaking translational symmetry[1]. Much of the reason for the current interest in such states derives from observations that unconventional superconductivity tends to emerge in materials exhibiting competing ground states with different broken symmetries, including nematic, charge, and/or spin density wave fluctuations[2–6]. However, disentangling the effects of quantum critical nematic fluctuations from other competing order parameter fluctuations presents a significant challenge. Moreover, the emergence of superconductivity preempts the low temperature behavior where a quantum phase transition may be present. Hence there is an interest to investigate electronic nematicity on its own, without the presence of competing phases.

Ferroquadrupolar order of atomic orbitals is an important realization of electronic nematicity, in which electronic orbitals spontaneously develop quadrupole moments oriented in the same direction[7,8]. Coupling between the quadrupolar moments and the lattice gives rise to an effective interaction between the atomic orbitals, and leads to a cooperative Jahn-Teller distortion at a temperature, T_Q[9]. In many cases ferroquadrupolar order develops in insulators, without the presence of competing broken symmetry phases. $TmVO_4$ is an ideal example of such a material, which has been well characterized[10,11]. The Tm ions ($4f^{12}$ with $L = 5$, $S = 1$, $J = 6$) in this material have partially filled 4f shells that are split by a tetragonal crystal field. The ground state doublet is well separated by a gap of ~77 K to the lowest excited state[12]. Importantly, the ground state is a non-Kramers doublet, such that the first order Zeeman interaction vanishes for in-plane fields (i.e., $g_c \sim 10$ while $g_a = g_b = 0$). The ground state can be well-described by a pseudospin ($\tilde{S} = 1/2$), in which one component, $\tilde{S}_z$, corresponds to a magnetic dipole moment oriented along the *c*-axis, while the other two components $\tilde{S}_x$ and $\tilde{S}_y$ correspond to electric quadrupole moments with B_{2g} (xy) and B_{1g} ($x^2 - y^2$) symmetry respectively[13]. Quadrupole interactions dominate, and the material does not order magnetically. The two quadrupole moments couple bilinearly to objects that transform with the same symmetry, and hence such objects can act as effective fields for the quadrupole order. This could be strains $\varepsilon_{xx} - \varepsilon_{yy}$, ε_{xy} or it could be composite magnetic field variables that transform in the same way, such as $B_x^2 - B_y^2$ and B_xB_y, where x and y lie along the axes of the undistorted tetragonal unit cell (see Supplementary Information). Hence, although in-plane magnetic fields do not couple linearly to the quadrupole moments, they do couple quadratically, and (appropriately constructed objects that go as the square of the fields) can act as effective longitudinal and transverse fields for a quadrupole ordered state, respectively. In $TmVO_4$, the quadrupole moment of the doublet couples to the lattice strain, ε_{xy}, and the material spontaneously undergoes a tetragonal to orthorhombic distortion with B_{2g} symmetry below $T_Q = 2.15$ K with orthorhombicity $\delta \approx 0.01$. The low energy degrees of freedom can be described well by the transverse field Ising model, in which Ising interactions couple the pseudospins which represent the quadrupolar moments and a magnetic field along the *c*-axis couples transverse to the quadrupolar direction[7]. This field enhances the fluctuations of the pseudospins and can tune the system to an Ising-nematic quantum phase transition at a critical field $B_c \approx 0.5$ T[11]. This material thus offers an important platform to investigate quantum critical nematic fluctuations in an insulator.

The critical behavior of the ferroquadrupolar order has been well documented for fields along *c*-direction, but little is known about the behavior for in-plane magnetic fields. Although the in-plane Zeeman interaction vanishes to first order, the second order effect can become important for sufficiently high magnetic fields[14]. Nuclear Magnetic Resonance (NMR) is a technique that can probe nematicity locally through the magnetic and electronic charge environment to which the NMR-active nucleus couples

[1]Department of Physics and Astronomy, University of California Davis, Davis, CA, USA. [2]Max Planck Institute for Chemical Physics of Solids, D-01187 Dresden, Germany. [3]Geballe Laboratory for Advanced Materials and Department of Applied Physics, Stanford University, Stanford, CA 94305, USA. [4]Laboratoire National des Champs Magnétiques Intenses, LNCMI-CNRS (UPR3228), EMFL, Université Grenoble Alpes, UPS and INSA Toulouse, 38042 Grenoble, France. ✉email: njcurro@ucdavis.edu

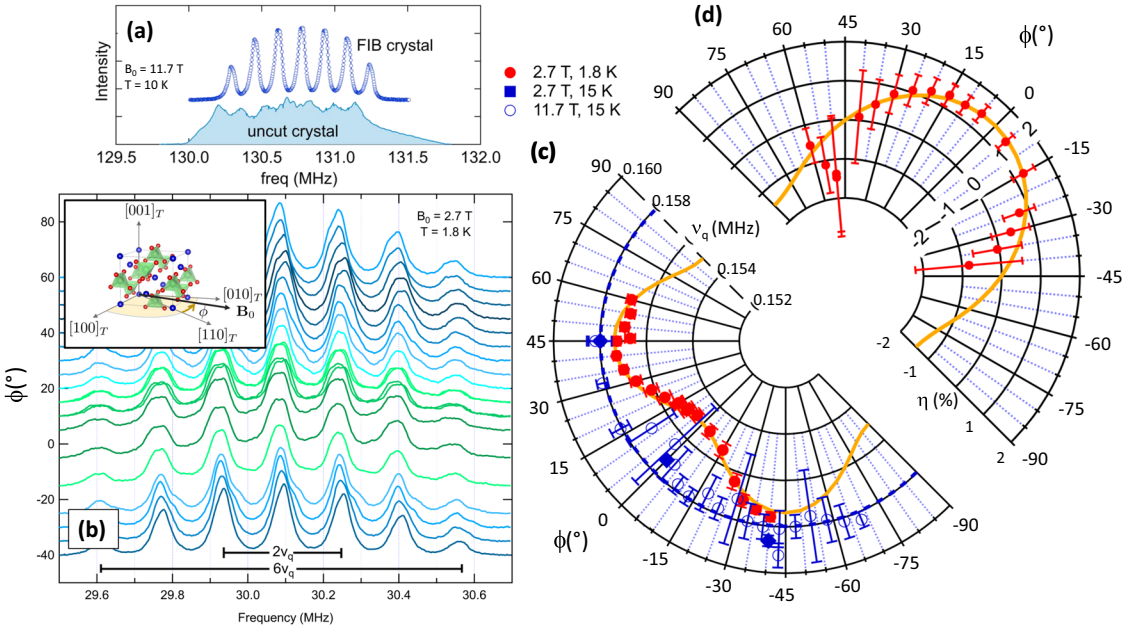

Fig. 1 NMR spectra for in-plane fields. a ^{51}V spectra of ellipsoidal (FIB) and uncut samples measured at T=10 K and B_0=11.7294 T oriented perpendicular to c, illustrating the broadening effect of the inhomogeneous demagnetization field on the seven nuclear spin transitions. **b** Spectra as a function of in-plane field angle, ϕ, measured at 2.7 T and 1.8 K. Colors correspond to ϕ modulo 90°. INSET: Diagram of field orientation with respect to the tetragonal unit cell, with the angle ϕ being measured from the $[110]_T$ direction. Blue atoms are Tm, green are V, and red are oxygen. **c** Polar plot showing the average quadrupolar splitting, ν_q, as a function of in-plane angle, ϕ, at 2.7 T and 1.8 K (solid red circles), 2.7 T and 15 K (solid blue squares) and 11.7 T and 15 K (open blue circles). The solid yellow line is a fit as described in the text, and the dashed line is a guide to the eye assuming tetragonal symmetry with no in-plane anisotropy ($\eta = 0$). **d** The ϕ-dependence of η at $B = 2.7$ T and $T = 1.8$ K. The solid yellow line is given by $\eta(\phi) = \eta_0 \cos(2\phi)$ with $\eta_0 = 1.44\%$. Thus $\eta(\phi)$ switches sign from positive to negative as the field is rotated from 0° to 90°. Error bars are standard deviations.

through its spin and quadrupole moment, respectively. Quadrupolar fluctuations are a measure of the nematic susceptibility and contribute to the spin–lattice relaxation rate T_1^{-1}, but have to be neglected usually when magnetic fluctuations dominate the relaxation. Recovering the quadrupolar relaxation is of particular interest in measurements of the iron-based superconductors, as their putative nematic quantum critical point appears to be correlated with optimal superconductivity and non-Fermi-liquid behavior in the normal state, indicating a possible role for nematic fluctuations in the pairing interaction[15–18].

Previous NMR measurements of $TmVO_4$ identified a scaling between the spin–lattice relaxation rate and the shear elastic stiffness constant, c_{66}, suggesting that the ^{51}V ($I = 7/2$) nuclear spins couple to the Tm orbitals through the electric field gradient (EFG), giving rise to a quadrupolar relaxation channel[19]. However, the spectra were significantly broadened by inhomogeneous demagnetization fields and the anisotropic g-factor of the Tm ground state doublet. In order to better discern the spectra and relaxation mechanisms at play, we utilized a focused ion beam (FIB) to shape a single crystal of $TmVO_4$ in an ellipsoidal shape, with a homogeneous demagnetization field. This innovation provides enhanced spectral resolution that enables detailed in-plane angular-dependent studies. We find that the EFG asymmetry parameter, η, which is a direct measure of the ferroquadrupolar order parameter, depends sensitively on the direction of the in-plane magnetic field. We interpret this behavior as a consequence of a second order Zeeman effect on the non-Kramers doublets, and demonstrate how an in-plane magnetic field, depending on the field angle, can act as either an effective longitudinal or transverse field for ferroquadrupole order to selectively enhance or suppress nematicity in $TmVO_4$. A further consequence of this innovation is that we have been able to disentangle the magnetic and quadrupolar contributions to the V spin–lattice relaxation. We find these rates exhibit different temperature dependencies, and depend not only on the orientation of the applied magnetic field in the ab plane, but also vary strongly with applied field strength. Surprisingly, we find that for transverse in-plane fields, T_Q is enhanced for applied fields $0 \leq B \lesssim 5$ T. This unusual behavior may reflect the influence of the excited crystal field states. For fields greater than ~5 T, the phase transition appears to exhibit a crossover rather than suppress to zero. We speculate that this behavior is related to the dynamics of isolated two-level systems once the magnetic field is sufficiently large to split the Tm ground state doublets. These unexpected observations for in-plane fields reveal rich new physics driven by nonlinear Zeeman interactions in this model system.

RESULTS

Electric field gradient

^{51}V NMR spectra and relaxation rate measurements were conducted in a single crystal shaped by a plasma focused ion beam (FIB) as a function of temperature and magnetic field oriented in the plane perpendicular to the c-axis (see Methods). Figure 1a compares spectra of an as-grown single crystal with that from a FIB-shaped crystal, and Fig. 1b displays spectra as a function of in-plane field direction below T_Q at $\theta = 90°$ at 1.8 K and 2.7 T. There are seven transitions at frequencies given by $\nu_n = \gamma B_0(1 + K) + n\nu_q$, where $\gamma = 11.193$ MHz/T is the gyromagnetic ratio, K is the magnetic shift ($\approx -0.4\%$), $n = -3, \cdots, +3$, and ν_q is the quadrupolar shift that arises due to the electric field gradient (EFG) tensor. The ϕ dependence of ν_q is determined by the EFG asymmetry parameter, $\eta \propto \varepsilon_{xy}$, where ε_{xy} is the B_{2g} strain in the ordered state (see Methods). As seen in Fig. 1c, ν_q exhibits fourfold, rather than twofold, symmetry at 1.8 K, in contrast to the expectation. Moreover, the spectra in Fig. 1 reveal only one set of peaks below 2 K, suggesting that there is a single nematic domain. These observations suggest the presence of a magnetoelastic

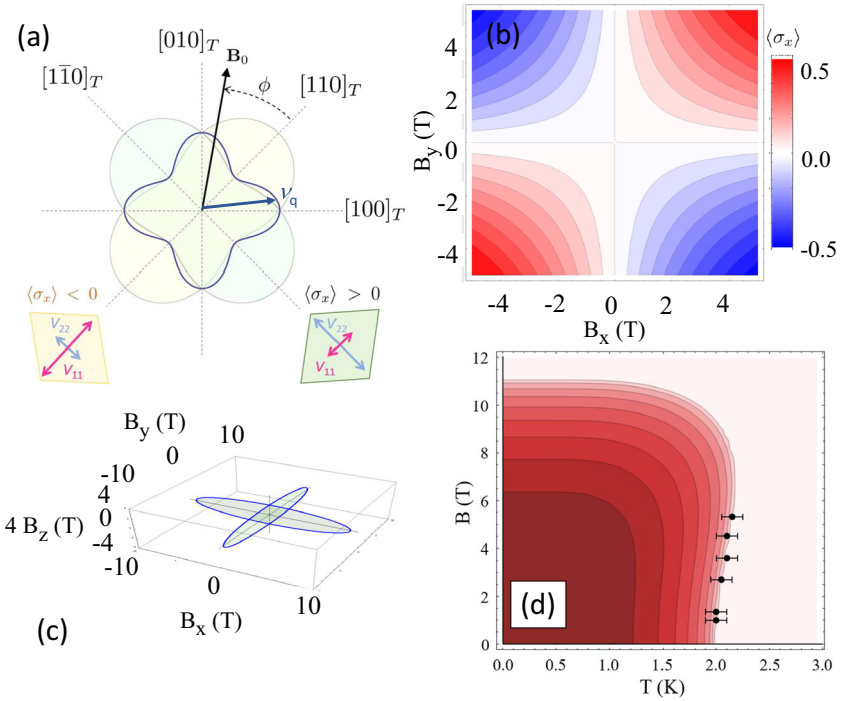

Fig. 2 Effect of in-plane fields on nematicity. a Polar plot of v_q as a function of field direction for constant $\eta > 0$ (green) and $\eta < 0$ (yellow). The thick blue line shows $v_q(\phi)$ with angular-dependent $\eta(\phi)$. The diamonds indicate the two domains with negative shear strain, ε_{xy} (order parameter $\langle\sigma_x\rangle < 0$, yellow) and positive strain ($\langle\sigma_x\rangle > 0$, green). ϕ measures the angle relative to the $[110]_T$ direction in the tetragonal unit cell, such that $\phi = 0$ lies along the B_{2g} distortion direction. Note that $\eta \propto \varepsilon_{xy} \propto \langle\sigma_x\rangle$. **b** Longitudinal fields induce finite order above T_Q and smear out the phase transition. The ferroquadrupolar order parameter, $\langle\sigma_x\rangle$, is shown at $T = 4\ \mathrm{K} > T_Q$ as a function of field direction in the plane perpendicular to the *c*-axis. The order parameter vanishes only for $B_x = 0$ or $B_y = 0$. **c** Quantum critical field (blue) as a function of magnetic field direction. The two intersecting ellipses are in the $B_x - B_z$ and $B_y - B_z$ planes respectively. **d** Calculated phase diagram for the effective model given by Eq. (5) with $\xi = 0.002T^{-2}$. Light colors correspond to $\langle\sigma_x\rangle = 0$ and darker red corresponds to increasing values of $\langle\sigma_x\rangle$. Solid black circles correspond to the peaks indicated by the blue arrows in Fig. 3.

coupling such that $\mathbf{B}_0$ detwins the ferroquadrupolar order causing η to depend on the field direction. A similar phenomenon affects the nematicity in the iron-based superconductors[20]. If we assume $\eta = \eta_0 \cos(2\phi)$, then we are able to model the data in Fig. 1b with $\eta_0 = 1.44\%$, as shown in Fig. 1d and illustrated in Fig. 2a. This behavior suggests the Tm quadrupole moments rotate with $\mathbf{B}_0$, such that domains with positive shear strain are always lower in energy. The fact that $\eta(\phi)$ changes sign implies that the principal axes of the EFG switches, however we assign a fixed axis as the evolution of $v_q(\phi)$ is captured well by a smoothly varying asymmetry parameter, implying weak pinning of nematic domains. At low fields and temperatures we are able to accurately fit the full spectra for all orientations with two magnetic sites but equal EFG parameters. In principle, we might expect two sites with $\pm\eta$ corresponding to different nematic domains, at least for some angles. However, even if there were two sites with different η in the nematic phase in zero field, the magnetoelastic coupling lowers the free energy of one domain over the other, effectively giving a single EFG environment for $\phi \neq 45°$. Moreover, v_q is independent of η for $\phi = 45°$, so even if two nematic domains were present their spectra would overlap at this angle. The equal width for all satellites indicates that there is little to no inhomogeneity of the EFG parameters. This result indicates both that any variations of η between nematic domains, and the structural disorder due to any impurities, crystal defects and their associated strains, must be small.

Spin–lattice relaxation

^{51}V has both a nuclear magnetic moment and a nuclear quadrupolar moment ($Q = 52$ millibarn), and therefore both fluctuations of the hyperfine field and fluctuations of the EFG can give rise to spin–lattice relaxation. In a previous study we investigated the anisotropy of the nuclear spin–lattice relaxation rate and found evidence that fluctuations of the Tm quadrupoles may contribute to the nuclear spin–lattice relaxation via the EFG at the V site[19]. In general, there are three distinct relaxation channels: a magnetic, W_m, and two quadrupolar relaxation rates, W_{Q1} and W_{Q2}, but it is difficult to disentangle the contribution of each[21]. These relaxation channels couple different sets of the I_z nuclear spin levels. W_{Q1} corresponds to transitions between nuclear spin states, $|m\rangle$, such that $\Delta m = \pm 1$ and W_{Q2} corresponds to transitions such that $\Delta m = \pm 2$. Usually W_{Q1} and W_{Q2} increase at structural transitions when ionic or electronic charges fluctuate strongly, and their relative contribution depends on the symmetry of these fluctuations and the magnetic field orientation with respect to the principal axes of the EFG tensor. The relaxation measured at a particular nuclear spin transition $m \leftrightarrow (m-1)$ is a complicated function of W_m, W_{Q1} and W_{Q2} determined by a master equation (with an 8×8 dimensional matrix for spin 7/2 of ^{51}V), as discussed the Supplementary Materials. The relaxation function for each transition is slightly different, thus by measuring the relaxation at multiple transitions one can globally fit the set of seven recovery curves to extract W_m, W_{Q1} and W_{Q2}. However, in order to do so it is vital to resolve and excite each transition in the spectrum individually. The inhomogeneous broadening from the demagnetization field precluded such studies previously, but fortunately all seven transitions are clearly visible in the FIB sample. Figure 3a, b demonstrates that the relaxation measured at each of these transitions requires consideration of quadrupolar relaxation.

Figure 3c–f shows the field and temperature dependence of W_{Q1}/T and W_m/T obtained by global fits to all seven nuclear transitions. Note that we constrain $W_{Q2} = W_{Q1}/4$ for this

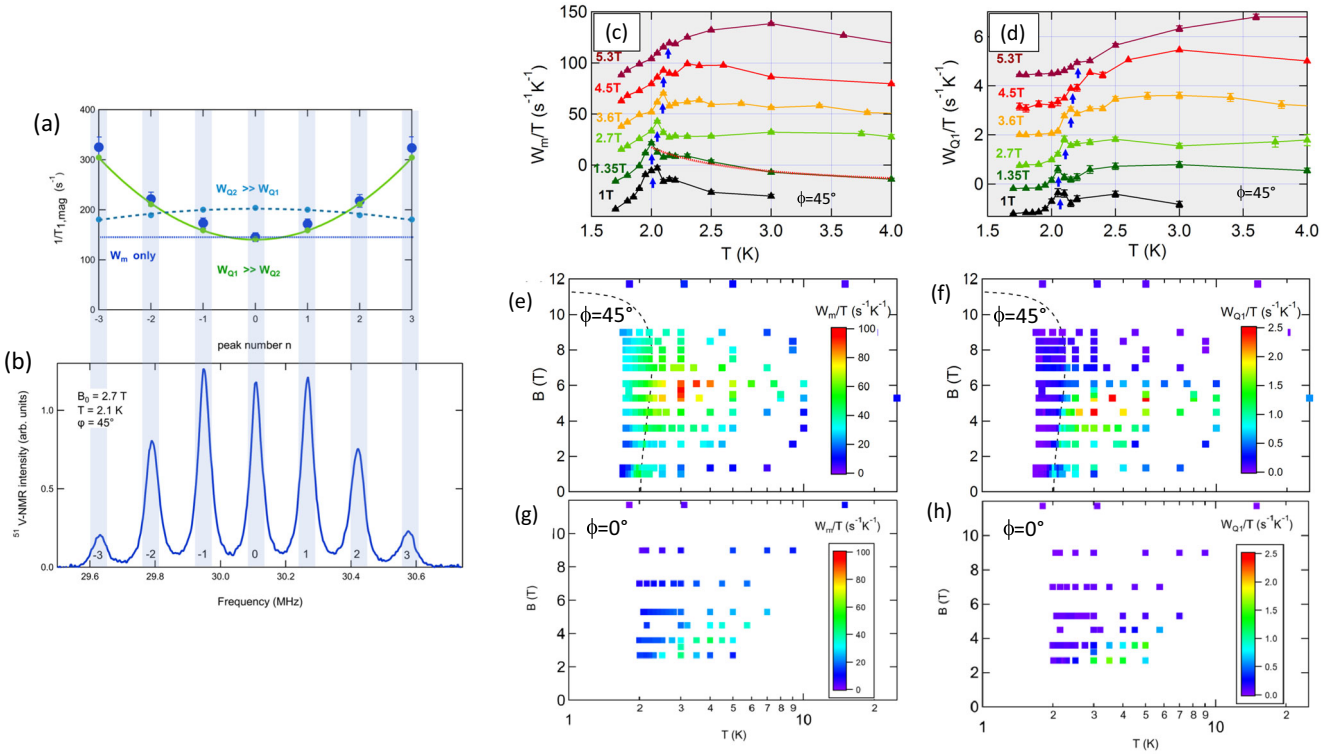

Fig. 3 Magnetic and quadrupolar relaxation rates for in-plane fields. a Plot of the magnetic relaxation rate $T_{1,\mathrm{mag}}^{-1} = 2W_m$ (large blue circles) with strongly enhanced relaxation rates on the outermost satellites ($n = \pm 3$) at $B_0 = 2.7$ T and $T = 2.1$ K. Purely magnetic relaxation should give identical $T_{1,\mathrm{mag}}^{-1}$ for all peaks (horizontal line). Fits to magnetic relaxation only of simulated relaxation curves that include $W_{Q1} = 2.3\ \mathrm{s}^{-1}$ and $W_{Q2} = 0$ reproduce the upward curvature of $T_{1,mag}^{-1}$. Inclusion of $W_{Q2} = 2.3\ \mathrm{s}^{-1}$, but $W_{Q1} = 0$ leads to downward curvature. Lines are quadratic fits and vertical bars link relaxation data with the corresponding transitions of the NMR spectrum. Error bars indicate standard deviations. **b** Spectrum of FIB sample at $B = 2.7$ T and $T = 2.1$ K. **c**, **d** The magnetic and quadrupolar relaxation rates divided by temperature, W_m/T and W_{Q1}/T, versus T for small fields along $\phi = 45°$. The data at each field have been displaced vertically for clarity. Blue arrows are guides to the eye indicating T_Q. The dotted red line is a fit to Eq. (3) as described in the text with $\Theta = 1.18$ K. Panels **e**, **f** show W_m/T and W_{Q1}/T plotted as heat maps over temperature and field. At low fields, sharp anomalies at $T_Q = 2.15$ K are visible and broaden and increase with increasing fields. Above B ~6 T both relaxation channels, especially W_{Q1}/T, are rapidly suppressed. The dashed lines in the background of panels (**c**, **d**) are guides to the eye based on the computed $T_Q(B)$ shown in Fig. 2d. Panels (**g**, **h**) show W_m/T and W_{Q1}/T for the longitudinal direction $\phi = 0°$. Unlike the data for $\phi = 45°$, no sharp anomalies at $T_Q = 2.15$ K are visible and the relaxation rates are always smaller.

orientation for these fits[19]. These data were acquired for at $\phi =$ 45°, in which $\mathbf{B}_0$ is aligned transverse to the ferroquadrupolar distortion (see Fig. 2a). Figure 3g, h show the same data for the longitudinal direction $\phi = 0°$. Note that W_{Q1}/T and W_m/T are determined by the dynamical magnetic and nematic susceptibilities of the Tm 4f electrons:

$$\frac{W_m}{T} \sim \lim_{\omega \to 0} \sum_{\mathbf{q},\alpha,\beta} \mathcal{F}_{\alpha\beta}(\mathbf{q}) \frac{\mathrm{Im}\chi_{\alpha\beta}^{\mathrm{mag}}(\mathbf{q},\omega)}{\omega} \tag{1}$$

$$\frac{W_{Q1}}{T} \sim \sum_{\mathbf{q}} \frac{\mathrm{Im}\chi^{\mathrm{nem}}(\mathbf{q},\omega)}{\omega}, \tag{2}$$

where $\mathcal{F}_{\alpha\beta}(\mathbf{q})$ is the hyperfine form factor[19,22]. The dynamical magnetic and nematic susceptibilities, χ^{mag} and χ^{nem}, are likely coupled to one another and are driven by the fluctuations of the Tm quadrupolar moments. The details of the frequency dependence of the susceptibility and relaxation of the collective excitations, however, remain unclear. Qualitatively, we expect contributions to arise both from the dynamics of isolated doublets split by the Zeeman interaction and coupled to a bath of phonons[23], as well as the collective dynamics associated with the ferroquadrupolar ordering in the vicinity of T_Q[13].

For the lowest fields (down to 1.35 T), both W_{Q1}/T and W_m/T exhibit a relatively sharp peak at T_Q and are suppressed below in the ordered state. It is remarkable that even at low fields both rates show distinct behaviors although magnetic fluctuations could be expected to result mainly from quadrupolar fluctuations of the ground state doublet. The relaxation rate above T_Q can be fit to a Curie-Weiss expression:

$$\frac{W_m}{T} = \frac{C_0}{T - \Theta}. \tag{3}$$

with a Weiss temperature $\Theta/T_Q = 0.55 \pm 0.13$, as shown by the dotted red line in Fig. 3c. This behavior likely reflects the divergence of nematic susceptibility at the phase transition[15,22]. The fact that $\Theta/T_Q < 1$ indicates that the elastic coupling between the Tm 4f moments and the ε_{xy} lattice strain renormalizes the exchange interaction between the moments[15]. Although we fit the data to only a limited temperature range limiting the precision of the fit, the value we obtain is consistent with previous measurements of the lattice elastic constant, c_{66}[24].

With increasing field, the sharp feature shifts upwards in temperature, as shown by the blue arrows in Fig. 3c, d, and a large broad peak emerges around ~3 K. The peak temperature increases by ~0.2 K by 5.3 T, and then disappears below the broad peak. The behavior up to this field suggests that the transition temperature T_Q increases with field, in contrast to the expectation that transverse fields should suppress T_Q to zero monotonically. The enhancement we observe may reflect the influence of higher order crystal field levels, as discussed below. At higher fields, both W_{Q1}/T and W_m/T exhibit broad maxima around 3 K, and the

feature associated with T_Q disappears. The origin of this behavior is unknown, but may be related to a change in the dynamics of isolated two-level systems as the Zeeman interaction increases. It is unclear if the ferroquadrupolar ordering is suppressed, or the 3 K feature simply overwhelms the signature of the phase transition. For $B_0 \gtrsim 6$ T, both relaxation rates decrease with increasing field, and reach their low-field values by ~9 T. The peak at 6 T may reflect the critical in-plane field, B^*, which is close to the estimated value based on the CEF parameters as discussed above. For higher magnetic fields, the splitting of the doublets will exceed k_BT and the dynamics will be gapped out.

DISCUSSION

Although the in-plane g-factor is zero and the Zeeman interaction vanishes to first order[25], the admixture of excited crystal field levels gives rise to a second order Zeeman interaction[14]:

$$\mathcal{H}_Z = -\frac{(g_J\mu_B B)^2}{2}[a\hat{\sigma}_1 + b\cos(2\phi)\hat{\sigma}_x + c\sin(2\phi)\hat{\sigma}_y], \quad (4)$$

where $\hat{\sigma}_\alpha$ are the Pauli matrices, $g_J = 7/6$ is the Landé factor, B is the magnitude of the in-plane field, and ϕ is defined in the inset of Fig. 1a. The parameters a, b, and c can be determined by perturbation theory and depend on the crystal field levels of the Tm, as shown in[10]. Note that for $\phi = 0$ or 90° ($\mathbf{B}_0 \| [110]_T$) the magnetic field should act as an effective longitudinal field to the ferroquadrupolar order, wiping out the phase transition at T_Q. For $\phi = 45°$ ($\mathbf{B}_0 \| [100]_T$), the magnetic field acts as an effective transverse field, such that T_Q is suppressed, but the transition should remain sharp. Using the values $b = c = a/2 = 0.082\ \mathrm{K}^{-1}$ reported by Bleaney et al., we estimate that T_Q should be suppressed to zero at a critical in-plane field of $B^* \approx \sqrt{2T_Q/c}/g_J\mu_B \approx 9.2$ T along this direction. Note that for any other in-plane angles, the phase transition will be smeared out. Thus there exist two intersecting lines of quantum phase transitions as as function of field orientation, as illustrated in Fig. 2c.

The second order Zeeman interaction provides a natural explanation of the unusual magnetoelastic coupling observed in the spectra as a function of ϕ. For $B = 2.7$ T where the angular dependence of the EFG asymmetry parameter was measured (Fig. 1c), $b(g_J\mu_B B)^2/2 \approx c(g_J\mu_B B)^2/2 \sim 0.1 k_B T_Q$ thus the field should have a minimal effect on the ferroquadrupolar order. On the other hand, the Zeeman interaction should lower the energy of one domain over the other, giving rise to a field-induced detwinning in the ordered state and the observed anisotropy η. In other words, as the field is rotated from $\phi = 0$ to $\phi = 90°$, domains with positive $\langle\sigma_x\rangle$ will convert to domains with negative $\langle\sigma_x\rangle$, in a manner similar to ramping an external magnetic field from negative to positive in a ferromagnet, and illustrated in Fig. 2b. An important difference, however, is that any field component away from $\phi = \pm 45°$ or $\pm 135°$ will act as a longitudinal field, giving rise to a crossover rather than a sharp phase transition. Moreover, these fields will favor one domain over the other, leading to a single value of η, as discussed above.

The enhancement of T_Q in a magnetic field is surprising. A similar effect was observed in TmCd, a material that also experiences a cooperative Jahn-Teller effect with a phase transition at 3.16 K[26]. However, the phase transition in TmCd is first order, and the effect was explained as the influence of a longitudinal field that shifts the first order discontinuity in the order parameter to higher temperatures and eventually broadens into a crossover. The phase transition in $TmVO_4$ is second order, and the enhancement we observe occurs for transverse fields where the phase transition remains sharp. A possible explanation for this observation is that the quadrupole moment of the Tm ground state doublet is enhanced by the magnetic field. The excited crystal field states admix with the ground state doublet, such that the magnitude of the quadrupolar moment grows quadratically with field (see Supplemental Materials). As a result, the effective Hamiltonian for the Tm moments in transverse fields ($\phi = 45°$) becomes:

$$\mathcal{H}_{eff}(B) = -\sum_{i\neq j} J_{ij}E^2(B)\hat{\sigma}_{x,i}\hat{\sigma}_{x,j} - c\frac{(g_J\mu_B B)^2}{2}\hat{\sigma}_y \quad (5)$$

so B both enhances the effective coupling between the Tm moments as well as induces quantum fluctuations. The mean field phase diagram for this model is displayed in Fig. 2(d) for $\xi = 0.002\ \mathrm{T}^{-2}$. As B increases, T_Q initially rises by ~0.2 K around 8 T and is then suppressed to zero at a critical field ~11 T. The phase transition remains sharp for all fields. This model captures the enhancement of T_Q for small B observed in Fig. 3c, d.

The behavior at higher fields remains unexplained. The data in Fig. 3 reveal a broad peak emerging around 3 K for $B \gtrsim 4$ T that spans several K, and the sharp feature associated with T_Q at lower B disappears, so that it is not possible to track the phase transition to higher fields. It is possible that the relaxation dynamics are simply dominated by the behavior of isolated field-split doublets, such that the collective behavior of the Tm moments is not evident at these high fields. A similar broad peak appears for longitudinal fields, shown in Supplemental Fig. S4.

An alternative explanation is that there is a small misalignment from $\phi = 45°$. As seen in Eq. (4), such a misalignment would contribute to a longitudinal field that will smear out the transition. This effect would increase with field, such that the phase transition remains relatively sharp at low fields, but is broadened at higher fields. Note, however, that for fields in the range $2\ \mathrm{T} \lesssim B \lesssim 5$ T, W_m/T and W_{Q1}/T exhibit both a broad peak as well as a sharper feature at T_Q, suggesting two separate phenomena. The phase diagram for a misaligned field would not have two features, but rather a single phase transition that broadens and moves to higher temperatures with increasing field. Thus a misalignment is not fully consistent with our observations.

It is interesting to note that both the quadrupolar fluctuations (W_{Q1}/T) and the magnetic fluctuations (W_m/T) exhibit qualitatively similar trends with temperature and field in Fig. 3. This similarity suggests that the field-induced Tm moments are coupled with the Tm quadrupole moments, so that the critical fluctuations of the latter can drive fluctuations of the former. There are important differences between the two relaxation channels, however. For example, it is clear that W_{Q1}/T is more rapidly suppressed below T_Q than W_m/T. This observation suggests that W_{Q1}/T is a more direct measure of the freezing nematic fluctuations when the order parameter $\langle\sigma_x\rangle$ steeply grows below T_Q.

The exact mechanism that leads to the broad peak above T_Q at high fields remains unclear. Previous measurements indicate that the spin–lattice relaxation rate is correlated with c_{66} up to 100 K at 11.7 T, suggesting that nematic fluctuations dominate the relaxation of the V nuclei[19]. Our results are consistent with the previous measurements, but we have now disentangled the two relaxation channels. Both the previous and current measurements reveal the presence of the broad peak. A qualitative understanding of this peak may be that for temperatures $T > \Delta(B)/k_B$, where $\Delta(B)$ is the field-dependent splitting of the Tm doublet, the relaxation rate is determined by the growth of the nematic susceptibility as the lattice softens. On the other hand, for $T < \Delta(B)/k_B$, the fluctuations will be suppressed with decreasing temperature[23]. These two effects may conspire to give rise to the broad maximum when $T \sim \Delta(B)/k_B$, which itself is field-dependent. On the other hand, the angular dependence suggests something more than a local phenomenon. Comparison of NMR relaxation rates with other low-frequency dynamic probes, such as ultrasound attenuation, can be fruitful[27], however there is no report of ultrasound

experiments with fields applied in the plane to allow direct comparison.

Our study proposes a conceptually easy mechanism to identify and disentangle magnetic and quadrupolar relaxation rates. Since the seminal work of Suter et al. it has been generally assumed that standard relaxation rate measurements preclude accurate determinations of W_m, W_{Q1} and W_{Q2}[21], except in cases where ν_Q is sufficiently small that double-resonance experiments (SEDOR) can be performed[28,29]. However, as we show in $TmVO_4$, a deviation in the magnetic relaxation rates on two transitions, e. g. the central peak and an outermost satellite (see Fig. 3a, b), is a direct indication that quadrupolar mechanisms are at play. This could be complicated if satellites are broad in frequency and possess inhomogeneous relaxation rates across the peak, but valuable information about charge ordering could be extracted from the median relaxation rates extracted from stretched magnetic fits for different transitions in inhomogeneous systems such as cuprates like $La_{2-x}Sr_xCuO_4$[30,31]. This method is not directly applicable to the well-studied case of the nematic order in FeSe as both NMR active isotopes ^{57}Fe and ^{77}Se have no satellites since $I = 1/2$. However, $FeSe_{1-x}S_x$ could be an interesting material with ^{33}S having $I = 3/2$. Since the natural abundance is small such samples would need to be enriched with ^{33}S. It is expected that the relaxation rate of ^{33}S, $^{33}W_{Q1,2}/T$ will display a very different behavior than $(^{77}T_1T)^{-1}$, because in the former ^{33}S is sensitive to the divergent nematic susceptibility as the structural transition T_s is approached. Measurements of W_{Q1} and W_{Q2} above and below the superconducting T_c are a direct measure of interplay between superconductivity and nematicity as well as the importance of nematic fluctuations for the superconducting pairing. Related experiments have been performed in $BaFe_2(As_{1-x}P_x)_2$ by comparing relaxation rates of ^{75}As ($I = 3/2$) and ^{31}P ($I = 1/2$)[32], but the method described here allows a direct determination of W_{Q2}.

$TmVO_4$ is a model system for investigating nematic quantum criticality in an insulator, in which ferroquadrupolar ordering of Tm 4f orbitals is well-described by the transverse field Ising model for magnetic fields oriented along the crystalline c-axis[11]. The response to in-plane fields has not been previously investigated, because the Zeeman interaction for the Tm non-Kramers doublets vanishes to first order in this configuration. We have studied the ferroquadrupolar ordering for in-plane fields using NMR of a single crystal shaped by a FIB to eliminate inhomogeneous broadening effects, and uncovered pronounced in-plane anisotropy in the EFG and spin–lattice relaxation rates. By measuring the relaxation curves at multiple nuclear transitions of the ^{51}V nucleus, we disentangle magnetic and quadrupolar relaxation channels. We find that the phase diagram for in-plane fields is dominated by the second order Zeeman interaction, and that the in-plane magnetic field can act as an effective transverse or longitudinal field to the Ising-nematic order, depending on direction, and leads to a marked in-plane anisotropy in both relaxation channels. Also, we find that even for the case where the in-plane field corresponds to an effective transverse field, nevertheless small values of the magnetic field initially enhance the ferroquadrupolar ordering temperature before eventually suppressing the long-range order. This effect is tentatively ascribed to competing effects of field-induced mixing of higher energy crystal field eigenstates and the destabilizing effects of field-induced quantum fluctuations. For higher fields, the spin–lattice relaxation is dominated by a broad peak in temperature and field, which may be due to the dynamics of isolated doublets split by magnetic field. The second order Zeeman interaction also gives rise to a magnetoelastic coupling, so that as the magnetic field rotates in the plane, the nematic domains switch. Our results establish in-plane magnetic fields as a novel approach to tune $TmVO_4$ to a quantum phase transition, and also establishes an important new method to disentangle magnetic and quadrupolar relaxation channels for high spin nuclei in a variety of condensed matter systems. Our results also indicate that $TmVO_4$ should exhibit rich nonlinear magnetization effects for in-plane fields.

METHODS

Sample preparation

Single crystals of $TmVO_4$ were grown from a $Pb_2V_2O_7$ flux using 4 mole percent of Tm_2O_3, following the methods described in refs. [33,34]. The crystals grow as rectangular needle-like prisms, with the long-axis along the c-direction (see Supplemental Materials). The NMR spectrum depends sensitively on the shape of the crystal and the direction of the applied magnetic field, $\mathbf{B}_0$, which polarizes the magnetic moments and creates a magnetization $\mathbf{M}$ in the sample. Continuity of the flux-density $\mathbf{B} = \mu_0\mathbf{M} + \mathbf{B_0}$ across the sample surface requires a demagnetizing field $\mu_0\mathbf{H}_d$ in addition to $\mathbf{B}_0$[35]. In an arbitrarily shaped sample $\mu_0\mathbf{H}_d(\mathbf{r})$ and hence $\mathbf{B}(\mathbf{r})$ will be inhomogeneous and the NMR spectrum will be broadened because the nuclei each resonate at the local field[36]. In most cases this broadening is not sufficient to cause any significant problems for NMR, however in $TmVO_4$ the non-Kramers doublet has $g_c \approx 10$ and $g_{ab} = 0$. Although $\mathbf{B}_0$ can be oriented perpendicular to c, parts of the crystal near edges and corners tend to have components of $\mathbf{B}$ parallel to c, which exacerbates the broadening effect due to the large anisotropy of the susceptibility, χ. The resulting broadening is sufficient to wash out the quadrupolar splitting (~150 kHz) between the Tm satellites at low temperatures and high fields[19].

Focused ion beam

$\mu_0\mathbf{H}_d$ can be made homogeneous by cutting the sample in either a spherical or ellipsoidal shape[37]. For these studies we utilized a Xe^{2+} plasma focused ion beam (FIB) to cut our sample to an ellipsoid with the long-axis along the c-axis of the crystal[38]. The sample was cut from a carefully aligned cuboid from which calculated and programmed concentric circles are removed using by a xenon plasma FIB by Thermo Fisher Scientific with a 30 kV, 1 μA beam. Sample damage from the beam is only expected on the surface within a depth of 30–40 nm[39–41] and energy dispersive X-ray analysis (EDX) of a test surface verifies the unchanged composition of $TmVO_4$ below. The final sample diameter is 0.4 mm and the length of 1.3 mm require a total cutting time in excess of 25 h of each side. In the FIB process Al and C are deposited on the sample surface layer, however these do not affect the NMR signal from the bulk of the sample. The magnetic broadening was dramatically reduced in the FIB crystal, such that each of the seven peaks separated by the quadrupolar splitting are clearly resolved. The ability to resolve all seven peaks is important because it enables us to extract details of the magnetic and quadrupolar contributions to the spin–lattice relaxation rate that would otherwise be inaccessible, as discussed above in the section on Spin-lattice relation. For fields $B_0 \le 1.35$ T the broadening from demagnetizing fields is sufficiently reduced, so that a larger crystal whose sharp corners were carefully polished away by hand was utilized.

Crystal alignment

The sample was secured with superglue inside the coil to prevent motion due to torque arising from the anisotropic susceptibility. The coil was attached to a platform that was in turn inserted in a dual-axis goniometer (see Supplemental Materials). The crystal was aligned with $\mathbf{B}_0 \perp c$ by minimizing T_1^{-1}, and the in-plane orientation was controlled with a precision <0.1°[19].

Electric field gradient

To first order in the nuclear quadrupolar interaction, ν_q is given by:

$$\nu_q = \frac{\nu_{zz}}{2}\left[3\cos^2\theta - 1 + \eta\sin^2\theta\cos(2\phi)\right], \quad (6)$$

where $\nu_{zz} = eQV_{33}/12h$, $\eta = (V_{22} - V_{11})/(V_{11} + V_{22})$, and V_{ii} ($i = 1, 2, 3$) are the eigenvalues of the principal directions of the EFG tensor[42]. In the disordered tetragonal phase, we find that ν_q is independent of ϕ, reflecting the axial symmetry of the EFG where $V_{11} = V_{22}$ and $\eta = 0$. Below T_Q there is a small but discernible variation in ν_q as a function of ϕ. In this case $V_{11} \neq V_{22}$, and the principal directions of the EFG tensor lie along $[001]_T$ with eigenvalue V_{33}, along $[110]_T$ with eigenvalue V_{11}, and along $[1\bar{1}0]_T$ with eigenvalue V_{22}. Note that these axes lie at 45° with respect the high temperature tetragonal axes, as illustrated in Fig. 2a. Moreover, $\eta \propto \varepsilon_{xy}$, where ε_{xy} is the B_{2g} strain in the

ordered state. Fig. 1c displays ν_q as a function of ϕ above (blue) and below (red) T_Q. The spectra are fitted with Gaussian peaks and ν_q is determined from the average separation of the satellite peaks. Note that the separation of adjacent peaks is not exactly ν_q due to second order quadrupole shifts, however, the separation of corresponding high ($n > 0$) and low-frequency satellites ($n < 0$) are equal to $2n\nu_q$, as shown in Fig. 1b for illustration, so the average separation ν_q with the smallest error bars is determined based on the separation of all three pairs of satellites with $\pm n$: $\nu_q \equiv (\nu_1 - \nu_{-1} + \nu_2 - \nu_{-2} + \nu_3 - \nu_{-3})/12$. It can be seen that the T dependence of ν_q is weak at a particular orientation (namely $\phi = 45°$) for which ν_q is nearly identical at 1.8 K and 15 K. This behavior arises because the temperature dependence of ν_q comes primarily from $\eta(T)$, and $\cos(2\phi) = 0$ for $\phi = 45°$, allowing to identify the directions of the principal axes in the plane. The four-fold angular dependence observed for ν_q makes it impossible to distinguish between the V_{11} and V_{22} directions and consequently the angles $\phi = 0°$ and 90° are assigned arbitrarily.

DATA AVAILABILITY

All data needed to evaluate the conclusions are present in the paper and/or supplemental materials. Correspondence and requests for materials should be addressed to N.J.C.

Received: 26 January 2022; Accepted: 4 June 2022;
Published online: 27 June 2022

REFERENCES

1. Fradkin, E., Kivelson, S. A., Lawler, M. J., Eisenstein, J. P. & Mackenzie, A. P. Nematic fermi fluids in condensed matter physics. *Annu. Rev. Condens. Matter Phys.* **1**, 153–178 (2010).
2. Kivelson, S. A., Fradkin, E. & Emery, V. J. Electronic liquid-crystal phases of a doped Mott insulator. *Nature* **393**, 550–553 (1998).
3. Vojta, M. Lattice symmetry breaking in cuprate superconductors: stripes, nematics, and superconductivity. *Adv. Phys.* **58**, 699–820 (2009).
4. Fernandes, R. M., Chubukov, A. V. & Schmalian, J. What drives nematic order in iron-based superconductors? *Nat. Phys.* **10**, 97–104 (2014).
5. Baek, S.-H. et al. Orbital-driven nematicity in FeSe. *Nat. Mater.* **14**, 210–214 (2015).
6. Comin, R. & Damascelli, A. Resonant X-Ray scattering studies of charge order in cuprates. *Annu. Rev. Condens. Matter Phys.* **7**, 369–405 (2016).
7. Maharaj, A. V. et al. Transverse fields to tune an Ising-nematic quantum phase transition. *Proc. Natl Acad. Sci. USA* **114**, 13430–13434 (2017).
8. Rosenberg, E. W., Chu, J.-H., Ruff, J. P. C., Hristov, A. T. & Fisher, I. R. Divergence of the quadrupole-strain susceptibility of the electronic nematic system $YbRu_2Ge_2$. *Proc. Natl Acad. Sci. USA* **116**, 7232–7237 (2019).
9. Gehring, G. A. & Gehring, K. A. Co-operative Jahn-Teller effects. *Rep. Prog. Phys.* **38**, 1–89 (1975).
10. Bleaney, B. & Wells, M. R. Radiofrequency studies of $TmVO_4$. *Proc. R. Soc. A: Math. Phys. Eng. Sci.* **370**, 131–153 (1980).
11. Massat, P. et al. Field-tuned ferroquadrupolar quantum phase transition in the insulator $TmVO_4$. Preprint at arXiv: 2110.03791 (2021).
12. Knoll, K. D. Absorption and fluorescence spectra of Tm^{3+} in YVO_4 and YPO_4. *Phys. Status Solidi (B)* **45**, 553–559 (1971).
13. Melcher, R. L. The anomalous elastic properties of materials undergoing cooperative Jahn-Teller phase transisions. **12**, 1–77 (1976).
14. Washimiya, S., Shinagawa, K. & Sugano, S. Effective Hamiltonian for non-Kramers doublets. *Phys. Rev. B* **1**, 2976–2985 (1970).
15. Chu, J.-H., Kuo, H.-H., Analytis, J. G. & Fisher, I. R. Divergent nematic susceptibility in an iron arsenide superconductor. *Science* **337**, 710–712 (2012).
16. Kuo, H.-H., Chu, J.-H., Palmstrom, J. C., Kivelson, S. A. & Fisher, I. R. Ubiquitous signatures of nematic quantum criticality in optimally doped Fe-based superconductors. *Science* **352**, 958–962 (2016).
17. Lederer, S., Schattner, Y., Berg, E. & Kivelson, S. A. Enhancement of superconductivity near a nematic quantum critical point. *Phys. Rev. Lett.* **114**, 097001 (2015).
18. Maier, T. A. & Scalapino, D. J. Pairing interaction near a nematic quantum critical point of a three-band CuO_2 model. *Phys. Rev. B* **90**, 174510 (2014).
19. Wang, Z. et al. Anisotropic nematic fluctuations above the ferroquadrupolar transition in $TmVO_4$. *Phys. Rev. B* **104**, 205137 (2021).
20. Chu, J.-H. et al. In-plane electronic anisotropy in underdoped $Ba(Fe_{1-x}Co_x)_2As_2$ revealed by partial detwinning in a magnetic field. *Phys. Rev. B* **81**, 214502 (2010).
21. Suter, A., Mali, M., Roos, J. & Brinkmann, D. Mixed magnetic and quadrupolar relaxation in the presence of a dominant static Zeeman Hamiltonian. *J. Phys. Condens. Matter* **10**, 5977 (1998).
22. Dioguardi, A. P. et al. NMR evidence for inhomogeneous nematic fluctuations in $BaFe_2(As_{1-x}P_x)_2$. *Phys. Rev. Lett.* **116**, 107202 (2016).
23. Leggett, A. J. et al. Dynamics of the dissipative two-state system. *Rev. Mod. Phys.* **59**, 1–85 (1987).
24. Melcher, R. L., Pytte, E. & Scott, B. A. Phonon instabilities in $TmVO_4$. *Phys. Rev. Lett.* **31**, 307–310 (1973).
25. Griffith, J. S. Spin Hamiltonian for even-electron systems having even multiplicity. *Phys. Rev.* **132**, 316–319 (1963).
26. Lüthi, B., Mullen, M. E., Andres, K., Bucher, E. & Maita, J. P. Experimental investigation of the cooperative Jahn-Teller effect in TmCd. *Phys. Rev. B* **8**, 2639–2648 (1973).
27. Frachet, M. et al. High magnetic field ultrasound study of spin freezing in $La_{1.88}Sr_{0.12}CuO_4$. *Phys. Rev. B* **103**, 115133 (2021).
28. Suter, A., Mali, M., Roos, J. & Brinkmann, D. Separation of quadrupolar and magnetic contributions to spin–lattice relaxation in the case of a single isotope. *J. Magn. Reson.* **143**, 266–273 (2000).
29. Suter, A., Mali, M., Roos, J. & Brinkmann, D. Charge degree of freedom and the single-spin fluid model in $YBa_2Cu_4O_8$. *Phys. Rev. Lett.* **84**, 4938–4941 (2000).
30. Mitrović, V. F. et al. Similar glassy features in the ^{139}La NMR response of pure and disordered $La_{1.88}Sr_{0.12}CuO_4$. *Phys. Rev. B* **78**, 014504 (2008).
31. Arsenault, A., Imai, T., Singer, P. M., Suzuki, K. M. & Fujita, M. Magnetic inhomogeneity in charge-ordered $La_{1.885}Sr_{0.115}CuO_4$ studied by NMR. *Phys. Rev. B* **101**, 184505 (2020).
32. Dioguardi, A. P. et al. NMR evidence for inhomogeneous nematic fluctuations in $BaFe_2(As_{1-x}P_x)_2$. *Phys. Rev. Lett.* **116**, 107202 (2016).
33. Feigelson, R. Flux growth of type RVO_4 rare-earth vanadate crystals. *J. Am. Ceram. Soc.* **51**, 538–539 (1968).
34. Smith, S. & Wanklyn, B. Flux growth of rare earth vanadates and phosphates. *J. Cryst. Growth* **21**, 23–28 (1974).
35. Blundell, S. *Magnetism in Condensed Matter* (Oxford Univ. Press, 2001).
36. Lawson, M. et al. Measurements of the NMR Knight shift tensor and nonlinear magnetization in URu_2Si_2. *Phys. Rev. B* **97**, 075138 (2018).
37. Osborn, J. A. Demagnetizing factors of the general ellipsoid. *Phys. Rev.* **67**, 351–357 (1945).
38. Moll, P. J. Focused ion beam microstructuring of quantum matter. *Annu. Rev. Condens. Matter Phys.* **9**, 147–162 (2018).
39. Eder, K. et al. A multi-ion plasma FIB study: determining ion implantation depths of Xe, N, O and Ar in tungsten via atom probe tomography. *Ultramicroscopy* **228**, 113334 (2021).
40. Kelley, R., Song, K., Leer, B. V., Wall, D. & Kwakman, L. Xe + FIB milling and measurement of amorphous silicon damage. *Microsc. Microanal.* **19**, 862–863 (2013).
41. Giannuzzi, L. & Smith, N. TEM specimen preparation with plasma FIB Xe + ions. *Microsc. Microanal.* **17**, 646–647 (2011).
42. Slichter, C. P. *Principles of Nuclear Magnetic Resonance* 3rd edn (Springer-Verlag, Berlin 1992).

ACKNOWLEDGEMENTS

We acknowledge helpful discussions with R. Fernandes, A. P. Mackenzie, T. Briol, B. Ramshaw, and V. Taufour for susceptibility measurements. Work at UC Davis was supported by the NSF under Grants No. DMR-1807889 and PHY-1852581, as well as the UC Laboratory Fees Research Program ID LFR-20-653926. Crystal growth performed at Stanford University was supported by the Air Force Office of Scientific Research under award number FA9550-20-1-0252. P.M. was partially supported by the Gordon and Betty Moore Foundation Emergent Phenomena in Quantum Systems Initiative through Grant GBMF9068. M.D.B. acknowledges partial support from the Swiss National Science Foundation under project number P2SKP2 184069, as well as from the Stanford Geballe Laboratory for Advanced Materials (GLAM) Postdoctoral Fellowship program.

AUTHOR CONTRIBUTIONS

N.J.C. planned the project; P.M., M.D.B., and I.R.F. synthesized, characterized, and prepared the single crystals; K.R.S. performed the FIB process; I.V. performed the NMR measurements with assistance from Z.W. and T.K.; D.G. performed studies and calculations of the demagnetization effects, and I.V. performed the fitting and analysis of the data with assistance from M.H.; I.V., I.R.F., and N.J.C. wrote the manuscript with input from the other authors. All authors contributed to discussions of the results and interpretation.

COMPETING INTERESTS

The authors declare no competing interests.

ADDITIONAL INFORMATION

Supplementary information The online version contains supplementary material available at https://doi.org/10.1038/s41535-022-00475-1.

Correspondence and requests for materials should be addressed to N. J. Curro.

Reprints and permission information is available at http://www.nature.com/reprints

Publisher's note Springer Nature remains neutral with regard to jurisdictional claims in published maps and institutional affiliations.